catalysts

MDPI

Article

Sulfur Poisoning Effects on Modern Lean NO_x Trap Catalysts Components

Jesus Emmanuel De Abreu Goes [1,2], Annika Kristoffersson [1] and Louise Olsson [2,*]

[1] Volvo Cars, SE-405 31 Gothenburg, Sweden; jesus.emmanuel.de.abreu.goes@volvocars.com (J.E.D.A.G.); annika.kristoffersson@volvocars.com (A.K.)
[2] Competence Centre for Catalysis, Chemical Engineering, Chalmers University of Technology, SE-412 96 Gothenburg, Sweden
* Correspondence: louise.olsson@chalmers.se

Received: 29 April 2019; Accepted: 24 May 2019; Published: 28 May 2019

Abstract: In the present work, a series of different materials was investigated in order to enhance the understanding of the role of modern lean NO_x trap (LNT) components on the sulfur poisoning and regeneration characteristics. Nine different types of model catalysts were prepared, which mainly consisted of three compounds: (i) Al_2O_3, (ii) Mg/Al_2O_3, and (iii) $Mg/Ce/Al_2O_3$ mixed with Pt, Pd, and Pt-Pd. A micro flow reactor and a diffuse reflectance infrared Fourier transform spectrometer (DRIFTS) were employed in order to investigate the evolution and stability of the species formed during SO_2 poisoning. The results showed that the addition of palladium and magnesium into the LNT formulation can be beneficial for the catalyst desulfation due mainly to the ability to release the sulfur trapped at relatively low temperatures. This was especially evident for $Pd/Mg/Al_2O_3$ model catalyst, which demonstrated an efficient LNT desulfation with low H_2 consumption. In contrast, the addition of ceria was found to increase the formation of bulk sulfate species during SO_2 poisoning, which requires higher temperatures for the sulfur removal. The noble metal nature was also observed to play an important role on the SO_x storage and release properties. Monometallic Pd-based catalysts exhibited the formation of surface palladium sulfate species during SO_2 exposure, whereas Pt-Pd bimetallic formulations presented higher stability of the sulfur species formed compared to the corresponding Pt- and Pd-monometallic samples.

Keywords: lean NO_x traps; sulfur poisoning; platinum; palladium; magnesium; ceria

1. Introduction

Stringent exhaust gas emission and fuel economy regulations, such as the European Real Driving Emission (RDE) and US Tier 3, have encouraged the development of advanced lean burn gasoline and diesel engines for their improved fuel economy and reduced greenhouse gas emissions. The implementation of these engines are, however, constrained by the need of catalytic systems in their lean exhaust to control the nitrogen oxide (NO_x) emissions. Current NO_x reduction technologies, such as NO_x storage and reduction (NSR; also known as lean NO_x trap, LNT), and selective catalytic reduction (SCR), are indeed expected to require more efficient NO_x abatement materials and strategies to cope with these regulations.

Lean NO_x trap is an effective NO_x reduction strategy able to attain high NO_x conversions over a wide range of temperatures without the need of additional on-board reductants [1,2]. It can also be used in combination with SCR catalysts to achieve low NO_x emissions. In fact, the combination of a close-coupled LNT and downstream SCR catalysts has been considered crucial to meet the forthcoming NO_x emission regulations [3]. The LNT catalyst complements SCR performance at low operating temperatures, and produces ammonia during the rich regeneration phase that can partially replace

urea [4]. Nevertheless, the LNT system is highly susceptible to sulfur, and its performance can be severely affected as NO_x storage sites are blocked by sulfur [5–7]. Sulfates formed on the NO_x storage sites have higher thermal stability than nitrates and nitrites and, therefore, their decomposition needs very high temperatures and alternating rich/lean exhaust mixtures [8,9]. This does not only lead to higher fuel consumption due to regular desulfation events, but may also cause structural deactivation of the catalyst, such as sintering of precious metals and the formation of mixed oxides (e.g., $BaAl_2O_4$ for the reaction between Al_2O_3 and BaO at high temperatures), affecting the overall NO_x storage and reduction activity of the catalyst [10–12].

Therefore, the sulfur tolerance of modern LNT catalysts should be improved by replacing the NO_x trapping material with a component with lower affinity towards sulfation, and with enhanced desorption of sulfur species during regeneration. Barium is frequently employed as a storage material because of its high thermal stability, however, it is responsible for the major LNT catalyst deterioration due to its high affinity for sulfation [13]. Ji et al. [14] studied the incorporation of ceria to Ba-based LNT catalysts and determined to provide a positive impact on LNT performance in the presence of sulfur. Ceria was found to enhance sulfur tolerance of the LNT catalyst by storing sulfur species, which mitigates the sulfation of barium sites. Rohr et al. [13] however, determined that barium is selectively poisoned in the presence sulfur over alumina and ceria. This may be attributed to the less alkaline nature of Ce and Al_2O_3 compared to Ba, which might lower the ability of Ce and Al_2O_3 to store sulfur and, therefore, result in more severe sulfation of the Ba phase [15]. Nevertheless, the amount of S stored on non-Ba oxides can be anyhow significant, delaying the Ba sulfation [16]. In other studies, Kylhammar et al. investigated the effect of MgO addition on the sulfation and desulfation behavior. They reported that Al_2O_3-MgO-based samples form less stable sulfur species by releasing SO_x already below 500 °C. Other studies have shown that the addition of MgO can also enhance the NO_x trapping performance and minimize irreversible precious metal sintering upon severe thermal aging treatments [17–19]. Nevertheless, the sulfur poisoning and regeneration behavior on MgO-CeO_2-based LNT catalysts have not been investigated yet to the best of our knowledge. Additionally, there is very limited work done on the influence of the noble metal nature on the SO_x storage and release properties for MgO and MgO-CeO_2 materials.

In this study, a number of different LNT components is investigated as regenerable NO_x traps. This effort aims to enhance the understanding of the role of modern LNT materials on the sulfur poisoning and regeneration characteristics. We, therefore, studied different metal oxides that are sufficiently basic for NO_x storage, such as Al_2O_3, CeO_2, and MgO, but less basic than BaO in order to minimize the sulfur poisoning. Nine different types of model catalysts were prepared, which mainly consisted of three compounds: (i) Al_2O_3, (ii) Mg/Al_2O_3, and (iii) Mg/Ce/Al_2O_3 mixed with Pt, Pd, and Pt-Pd.

2. Results

2.1. NO_2-TPD Experiments

In order to investigate the stability of the formed nitrates, NO_2-temperature programmed desorption experiments were conducted over all samples according to the experimental procedure described earlier. Firstly, the NO and NO_2 profiles over the NO_2 adsorption and Ar flushing steps are presented in Figure 1. The data clearly indicates that the adsorption of NO_2 leads to NO release in the gas phase. The NO formation is most probably associated to both NO_2 disproportionation and NO_2 decomposition reactions, which are well known in the literature [20–23]. The formation of NO increases in the order of PGM-Al_2O_3 < Mg-Al_2O_3 < Mg-Ce-Al_2O_3, where PGM denotes precious group metal. This is most likely because of the increase of NO_2 storage sites available for the disproportionation reaction by introducing Mg and Ce into the catalyst formulation. Additionally, Table 1 summarizes the results of NO_2-TPD experiments over the NO_2 adsorption and Ar flushing steps, which includes the total NO_x adsorbed (Total NO_x Ads). The total amount of NO_x adsorbed was determined by

subtracting the cumulative outlet NO_x concentration over the NO_2 adsorption and Ar flushing steps from the total amount of NO_x introduced into the system over the same period of time. The amount of NO_x stored was slightly higher for PGM-Al_2O_3 samples compared with Mg-containing catalysts, which probably indicates that Mg can block Al sites, resulting in a reduced NO_x storage capacity.

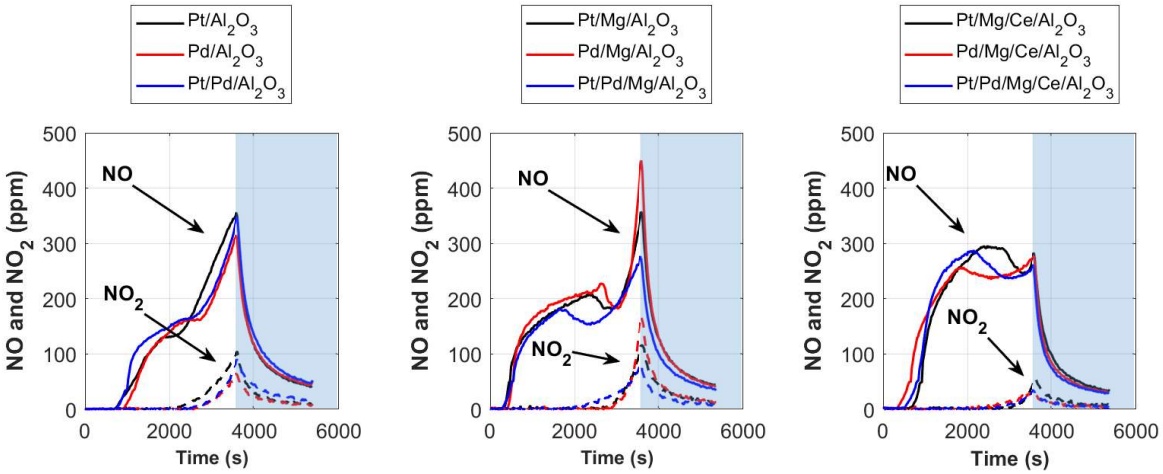

Figure 1. NO and NO_2 profiles over the NO_2 adsorption and Ar flushing (light blue) steps.

Table 1. Summary of TPD experiment for all samples tested: total amount of NO_x adsorbed, amount of NO and NO_2 desorbed during temperature ramp, and the temperature at 20% (T20) and 90% (T90) of NO_x released.

Sample	Total NO_x Ads (μmol)	NO Des. (μmol)	NO_2 Des. (μmol)	T20 NO_x (°C)	T90 NO_x (°C)
Pt/Al_2O_3	37.3	13.8	18.2	141	417
Pd/Al_2O_3	38.9	15.6	18.1	146	417
$Pt/Pd/Al_2O_3$	37.2	11.9	20.8	132	406
$Pt/Mg/Al_2O_3$	35.3	15.4	11.5	142	438
$Pd/Mg/Al_2O_3$	34.5	15	11.5	142	435
$Pt/Pd/Mg/Al_2O_3$	37.1	17.3	10	160	442
$Pt/Mg/CeO_2/Al_2O_3$	35.5	16.6	9.4	165	424
$Pd/Mg/CeO_2/Al_2O_3$	35.8	16.8	8.7	191	435
$Pt/Pd/Mg/CeO_2/Al_2O_3$	36	17	7.5	184	428

Regarding the desorption temperature, Table 1 numerically summarizes the results over the TPD step, containing the amount of NO and NO_2 desorbed, and temperature at 20% (T20) and 90% (T90) of NO_x released. Note that the total amount of NO (NO Des.) and NO_2 (NO_2 Des.) desorbed over the TPD step is slightly lower than the total NO_x adsorbed during NO_2 adsorption and Ar flushing steps (see Table 1). This could be because of temperature variations in the mass-spectrometer during the temperature ramping, leading to small experimental deviations. Moreover, Figure 2 shows the NO, NO_2, and total NO_x profiles as a function of the catalyst temperature. The total NO_x profiles are particularly used to properly assign the NO_x desorption peaks to their corresponding components, and compare their magnitudes with other catalyst groups. Clear differences in NO_x desorption profiles are presented, which suggests that the LNT formulation certainly influence the NO_x storage stability. Two NO_x desorption peaks were evident for PGM-Al_2O_3 samples, with their maximum approximately at 130 and 330 °C, respectively. Note that the magnitude of the low temperature maxima is slightly larger compared to the high temperature peak. The low temperature peak could be attributed to the removal of weakly adsorbed N_2O_4 and $NO_2^{+\delta}$ species, whereas the high temperature desorption peak could be associated to the decomposition of nitrate species from alumina sites [24,25]. Mg-Al_2O_3 samples show a similar TPD-profile with an additional peak located around 380 °C, ascribed to the decomposition of NO_x stored on magnesium sites [26]. The TPD spectra of Mg-Ce-Al_2O_3 samples in contrast show a shoulder around 160 °C and two intense peaks located around 330 and 380 °C,

respectively. Thereby, the results suggest that the presence of Mg and Ce into the LNT formulation certainly impact the stability of NO_x stored species. In fact, PGM-Mg-Al_2O_3 and PGM-Mg-Ce-Al_2O_3 samples presented up to 36 °C higher T90 temperatures compared to PGM-Al_2O_3 samples (see Table 1). This is most likely due to the formation of more strongly bound nitrate species in presence of Mg and Ce compared to PGM-Al_2O_3 samples [25,26]. Moreover, most of the NO_x stored was desorbed as NO for PGM-Mg-Al_2O_3 and PGM-Mg-Ce-Al_2O_3 samples because of the NO_2 dissociation at high temperatures (above 350 °C) over noble metal sites [27]. It should also be noted that the experiments do not emphasize a considerable impact of the precious metals used on the nature and amount of the NO_x released.

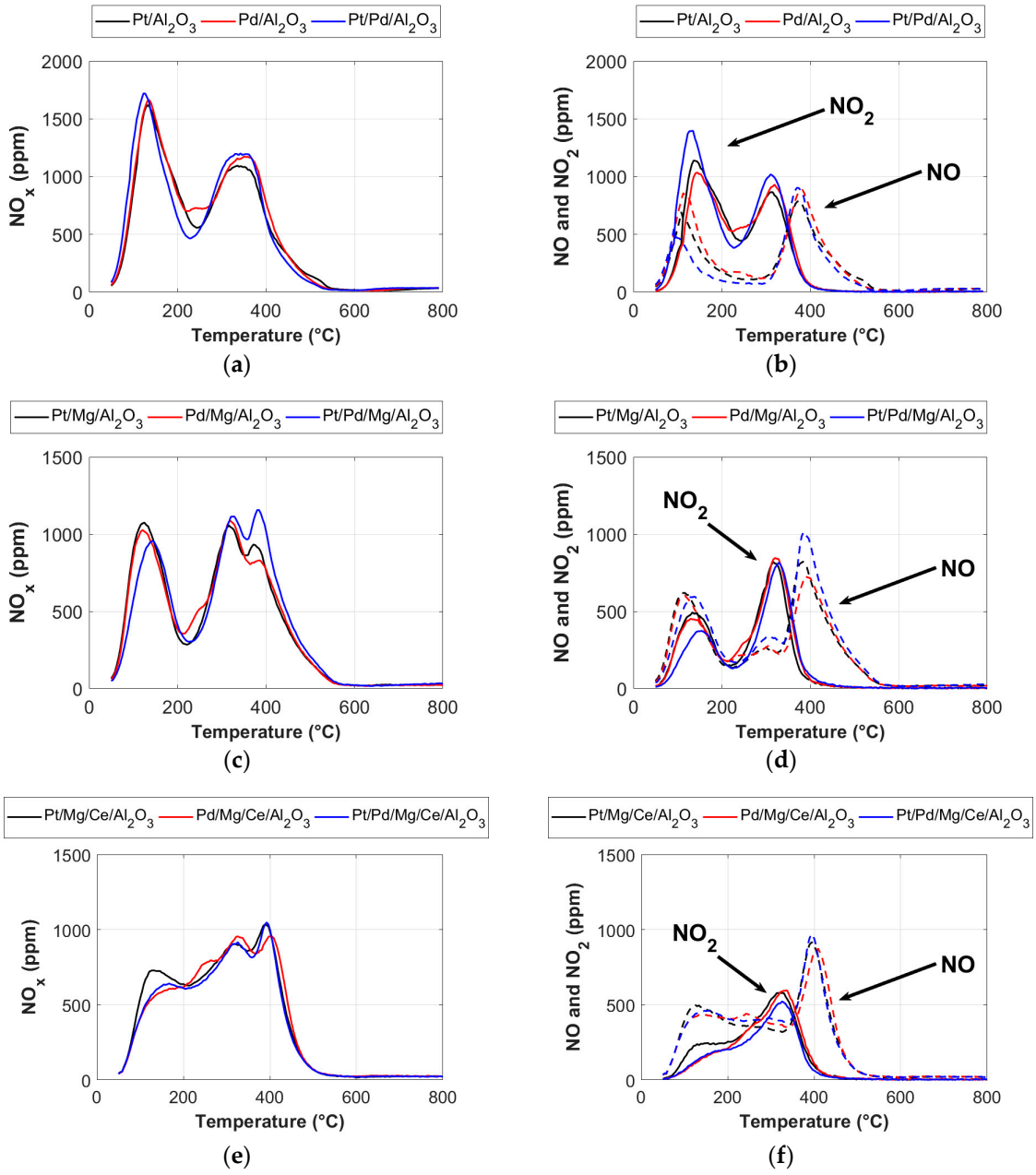

Figure 2. NO_x release as a function of the catalyst temperature during the TPD experiment for all samples. The total NO_x release profile is shown on the left, while the NO_2 and NO release profiles are shown on the right for the same group of samples. (**a**,**c**,**e**) show the total NO_x profiles, while (**b**,**d**,**f**) show the NO and NO_2 profiles for PGM-Al_2O_3, Mg-Al_2O_3 and Mg-Ce-Al_2O_3 groups of samples, respectively.

2.2. Sulfur Adsorption Characteristics—DRIFTS Experiments

The sulfation behavior of modern LNT compounds are discussed in this section, including the effects of SO_x poisoning on precious metals, magnesium, and cerium compounds. The sulfation mechanism was studied through DRIFT spectroscopy experiments.

2.2.1. Influence of Sulfur on Different Precious Metal Species

The mechanism of SO_x adsorption over LNT compounds was studied by DRIFT spectroscopy. Figure 3 shows the DRIFTS spectra of Pt/Al_2O_3, Pd/Al_2O_3, and $Pt/Pd/Al_2O_3$ samples after the exposure to 50 ppm SO_2 and 8% O_2 for 2 h at 200 °C in the range from 1100–1700 cm^{-1}. The spectrum presented represent a subtraction between the reference spectra recorded after pre-treatment at 200 °C and the spectra taken during the SO_x storage period. The corresponding spectra for Pt/Al_2O_3 show a substantial increase in the intensity of absorbed sulfur species on alumina. The band at 1352 cm^{-1} was quickly formed after 30 min of SO_2 exposure with a weak shoulder at 1386 cm^{-1}. Both absorbance bands were assigned to the formation of surface aluminum sulfate species [13,28,29]. These bands increased in intensity and shifted to higher frequencies with extended SO_2 exposure. The observed shift has been previously reported by several authors [30–32], ascribed to either pure frequency shift of a single band caused by the change in the strength of molecular interactions or the combined effect of two overlapping bands that differ in relative intensity. The shift in frequency is observed only after 90 min of sulfur poisoning. In this case, we therefore suggest that the resultant increase in frequency of the band at 1352 cm^{-1} is induced by the formation of bulk aluminum sulfate species, centered approximately at 1362 cm^{-1}, overlapping the surface aluminum sulfate band. Furthermore, a shoulder appeared approximately at 1297 cm^{-1} attributed to chemisorbed molecular SO_2 on alumina [33,34], and SO_3 on Pt [35]. The Pt/Al_2O_3 spectrum also has a wide band from ~1210 cm^{-1} to lower wavenumbers, which corresponds to the formation of bulk aluminum sulfate [34,36].

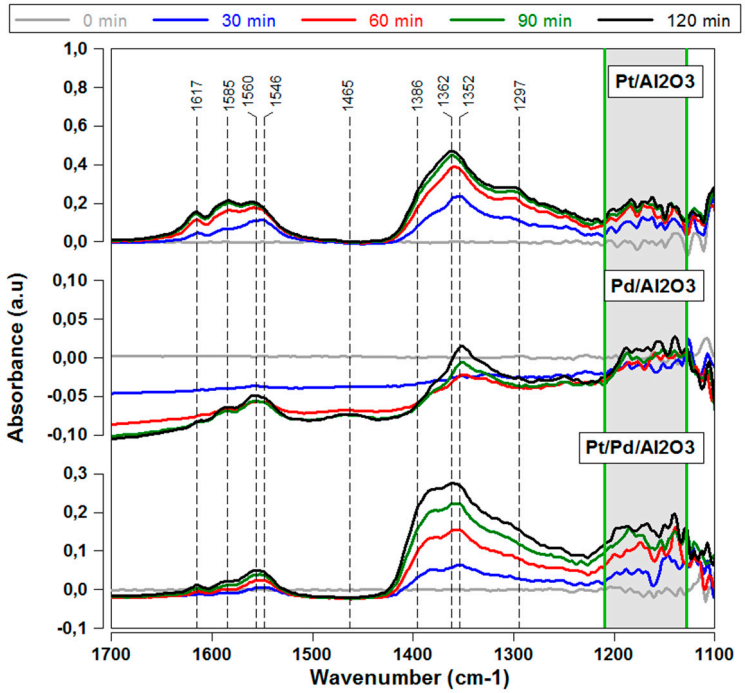

Figure 3. DRIFT spectra from 1100 to 1700 cm^{-1} for Pt/Al_2O_3, Pd/Al_2O_3, and $Pt/Pd/Al_2O_3$ samples after exposure to 50 ppm SO_2 and 8% O_2 at 200 °C for 0, 30, 60, 90, and 120 min. The blue band represents the frequency range for bulk aluminum sulfates formed over the samples tested (<1210 cm^{-1}).

The spectrum at high wave numbers obtained from the SO_2 exposure of Pd and Pt supported on Al_2O_3 is also shown in Figure 3. Similar to Pt/Al_2O_3 catalyst, the Pd/Al_2O_3 exhibit an intense band at 1352 cm^{-1} with a shoulder near 1386 cm^{-1}, both assigned to surface aluminum sulfate [29–31,34]. Likewise, bulk aluminum sulfate were also formed at lower wavenumber (<1200 cm^{-1}). Additionally, a weak absorbance band was shown around 1465 cm^{-1} after 2 h of SO_2 + O_2 exposure, which corresponds to sulfates formed on Pd sites [34,37–39]. This band was not observed for Pt/Al_2O_3 sample, which clearly indicates that monometallic Pd-based catalysts are more prone for sulfur poisoning than Pt sites. This is in agreement with previous investigations [40–43]. Lampert et al. [40] indeed reported an important increase in the activation energy after exposing Pd-based catalysts to sulfur species because of the formation of a $PdO\text{-}SO_3$ complex and, therefore, the decrease of the overall catalyst activity. On the contrary, these species apparently spill over rapidly from Pt sites to the alumina surface, which contribute to the resistance of Pt sites to sulfur poisoning [34]. Nevertheless, it is also well known that even the Pt-based catalysts eventually lost activity over time with exposure to sulfur [43].

From Figure 3, it is also clear that when $Pt/Pd/Al_2O_3$ sample was exposed to SO_2 under oxidizing conditions, surface aluminum sulfate species (1352, and 1386 cm^{-1}) were formed, in addition to bulk aluminum sulfates (<1210 and 1362 cm^{-1}). Furthermore, the absence of the peak at approximately 1465 cm^{-1} associated with $PdSO_4$ demonstrates that no stable sulfates are formed on Pd surface for Pt-Pd bimetallic samples under the conditions investigated. These results are consistent with the study by Sadokhina et al. [44], where $Pd/Pt/Al_2O_3$ was more resistant to sulfur poisoning compared to Pd/Al_2O_3 during methane oxidation.

Focusing on the hydroxyl region presented in Figure 4, all samples developed negative peaks at ~3760 and ~3727 cm^{-1}, in addition to a wide absorbance band from ~3660 cm^{-1} to lower wavenumbers. These peaks have been attributed to the interaction of SO_2 with hydroxyl groups on alumina (~3760 and ~3727 cm^{-1}) [29,34,45], and hydrogen-bounded sulfite species (<3660 cm^{-1}) [34]. Although no sulfites were observed for PGM-Al_2O_3 samples from the DRIFT spectra presented in Figure 3, it is suggested that the surface aluminum sulfates are also hydrogen-bonded to alumina OH–groups, producing the same effect on the OH stretching frequency [29]. Additionally, during SO_2 + O_2 exposure, all samples developed absorbance bands between 1540 and 1620 cm^{-1} (see Figure 3). These peaks are most likely attributed to the adsorption of different species over alumina, where the peak at 1617 cm^{-1} is particularly associated with water bound to the alumina surface as a result of the release of OH groups from the alumina surface [4,29,37]. The peaks developed between 1540 and 1585 cm^{-1} are attributed to the interaction of the weakly absorbed SO_2 species with Al^{n+} Lewis acid sites [46].

2.2.2. Influence of Sulfur on Magnesium Compound

Figure 5 shows the in situ DRIFTS spectra for $Pt/Mg/Al_2O_3$, $Pd/Mg/Al_2O_3$, and $Pt/Pd/Mg/Al_2O_3$ samples during the exposure to 50 ppm of SO_2 and 8% O_2 for 2 h at 200 °C. Similar spectrum were observed for all three samples, characterized predominantly by a broad band centered at 1098 cm^{-1}. This band can be attributed to asymmetric stretches of surface-bound SO_3 (sulfate) on MgO sites [6,47,48]. A second adsorption band is observed at 1346 cm^{-1} most probably due to the formation of surface aluminum sulfate [29,30,34]. Compared with the PGM-Al_2O_3 samples (see Figure 3), the intensity of the surface aluminum sulfate peak is low, indicating that only small amounts were formed. In fact, surface aluminum sulfate was primarily observed for $Pt/Mg/Al_2O_3$ and $Pt/Pd/Mg/Al_2O_3$ catalysts, whereas practically no surface aluminum sulfate could be identified for $Pd/Mg/Al_2O_3$ sample. This in turn means that the introduction of Mg in the LNT catalyst formulation leads to lower formation of surface aluminum sulfate. This can be attributed to the partial coverage of the Al_2O_3 surface with magnesium, and/or the higher affinity of Mg for S than Al_2O_3 [4,6,49]. Interestingly, the shoulder observed at 1297 cm^{-1} for PGM-Al_2O_3 samples did not evolve for Mg-Al_2O_3 catalysts, suggesting that Mg could prevent the formation of either chemisorbed molecular SO_2 on alumina or bulk aluminum sulfates during SO_2 exposure. In addition, $Pd/Mg/Al_2O_3$ sample showed weak bands at ~1462 and ~1637 cm^{-1}

assigned to palladium sulfates ($PdSO_4$) [34,37–39], and water bound to the catalyst surface (probably on alumina) [4,29,37], respectively. The latter was also weakly observed for the $Pt/Pd/Mg/Al_2O_3$ catalyst.

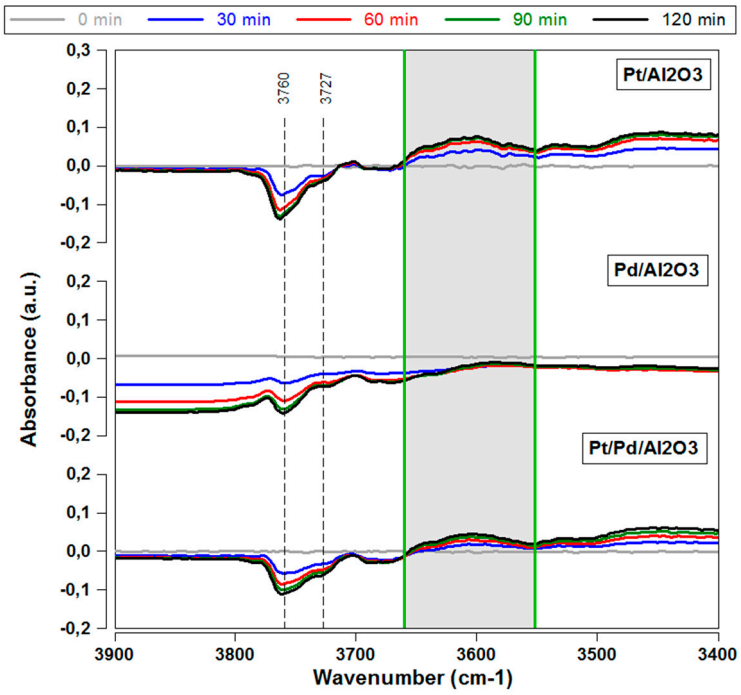

Figure 4. DRIFT spectra from 3400–3900 cm^{-1} for Pt/Al_2O_3, Pd/Al_2O_3, and $Pt/Pd/Al_2O_3$ samples after exposure to 50 ppm SO_2 and 8% O_2 at 200 °C for 0, 30, 60, 90, and 120 min. The blue band represents the frequency range for hydrogen-bounded sulfite species formed over the samples tested (<3660 cm^{-1}).

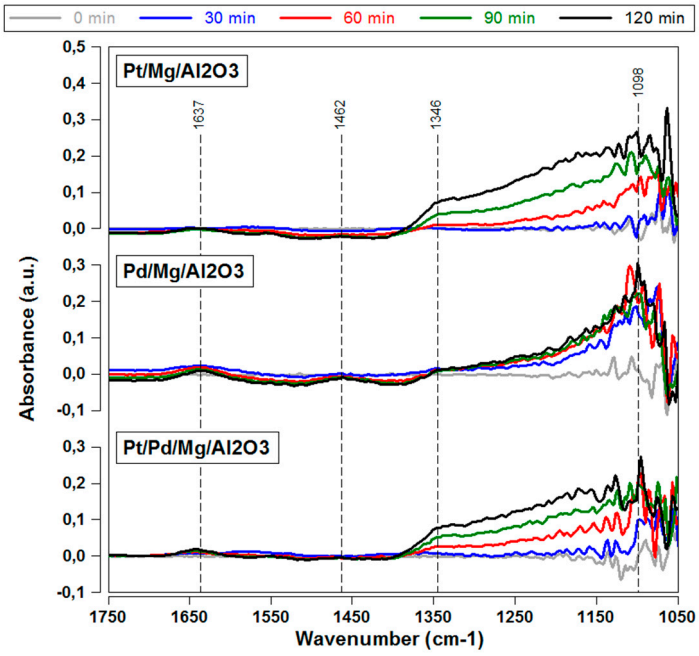

Figure 5. DRIFT spectra from 1000 to 1700 cm^{-1} for $Pt/Mg/Al_2O_3$, $Pd/Mg/Al_2O_3$, and $Pt/Pd/Mg/Al_2O_3$ samples after exposure to 50 ppm SO_2 and 8% O_2 at 200 °C for 0, 30, 60, 90, and 120 min.

2.2.3. Influence of Sulfur on Ceria Compound

In situ DRIFTS spectra as a function of time are presented in Figure 6 for Pt/Mg/Ce/Al_2O_3, Pd/Mg/Ce/Al_2O_3, and Pt/Pd/Mg/Ce/Al_2O_3 samples exposed to SO_2 + O_2 at 200 °C. Interestingly, Ce-Mg-Al_2O_3 samples showed relatively similar sulfated DRIFTS spectra compared with Mg-Al_2O_3 catalysts (see Figure 5). The primary differences are the more pronounced peak at 1346 cm^{-1} and the presence of a new adsorption band at 1156 cm^{-1}. According to the literature, the bands at 1346 and 1156 cm^{-1} correspond to surface and bulk sulfates [30,32,49,50], respectively. The surface sulfate can be either formed on Al_2O_3 and/or ceria sites [29,30,32,34,49], whereas bulk sulfate is mostly associated with ceria sites [32,49]. The 1156 cm^{-1} band can be also associated with bulk $MgSO_4$ [48], however, this is not likely since it was not observed for Mg-Al_2O_3 samples (see Figure 5). In addition, the band at 1098 cm^{-1} (for Mg-Al_2O_3) was slightly shifted to 1075 cm^{-1} for Ce-Mg-Al_2O_3 samples. This adsorption band can be assigned to the formation of surface magnesium and/or cerium sulfates. Note also that the bands at 1346 and 1075 cm^{-1} were quickly formed after 30 min of SO_2 exposure, whereas the adsorption band at 1156 cm^{-1} appeared only after 90 min when the band at 1075 cm^{-1} began to be saturated. This implies that in the presence of ceria, the sulfur starts to accumulate on the surface of the catalyst, and subsequently converts into bulk sulfate when the surface becomes saturated. This is in agreement with previous studies [38,51].

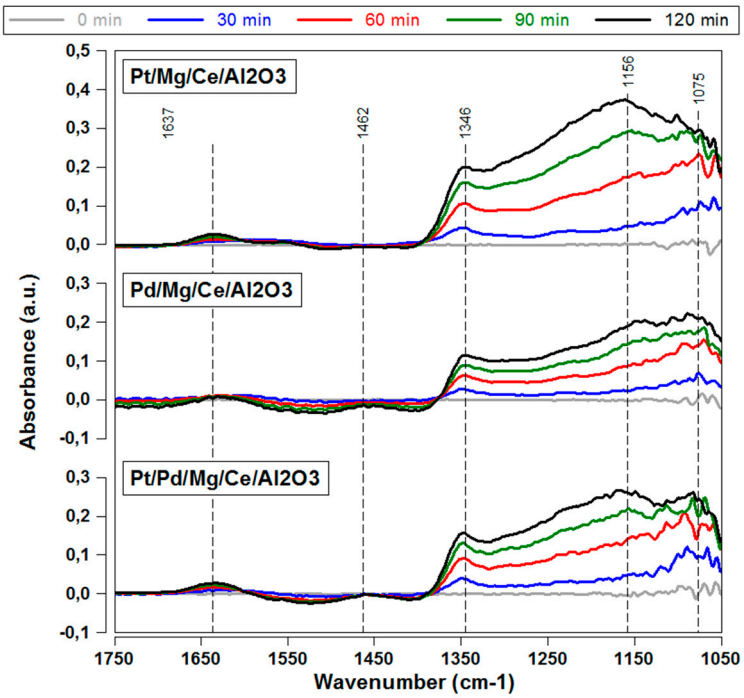

Figure 6. DRIFT spectra from 1000 to 1700 cm^{-1} for Pt/Mg/Ce/Al_2O_3, Pd/Mg/Ce/Al_2O_3, and Pt/Pd/Mg/Ce/Al_2O_3 samples after exposure to 50 ppm SO_2 and 8% O_2 at 200 °C for 0, 30, 60, 90 and 120 min.

2.2.4. Influence of Catalyst Temperature on SO_2 Poisoning

Identifying the stability of the sulfur species formed is crucial for an efficient desulfation event to recover the catalyst activity. Therefore, in order to better understand the stability of sulfur on various LNT components, DRIFTS spectra were collected from Pt/Al_2O_3, Pt/Mg/Al_2O_3, and Pt/Mg/Ce/Al_2O_3 samples during a temperature ramp. The samples were first exposed to 50 ppm of SO_2 and 8% O_2 for 2 h at 200 °C, and then the temperature was risen from 200 °C to 550 °C at a rate of 20 °C/min with the same feed composition (50 ppm of SO_2 and 8% O_2). Spectra were collected at each temperature and are presented in Figure 7, using a background spectrum taken before the SO_2 adsorption at 200 °C. An increase in intensity is clearly seen for all three samples as the temperature increases, in particular

the bands related to surface- and bulk-like sulfates. In fact, a new adsorption peak at ~1190 cm^{-1} was identified for $Pt/Mg/Al_2O_3$ at 550 °C, assigned to the formation of bulk $MgSO_4$ [48]. The bulk sulfate band indeed dominated the spectrum for Mg and Mg-Ce containing catalysts at 550 °C, indicating that both Mg and Ce play critical roles in increasing the sulfation for LNT catalysts. This is in good agreement with the results reported by Colussi et al. [38] and Boaro et al. [52]. Bulk sulfate bands were also shifted to higher wavenumbers by increasing the catalyst temperature, whereas, under such condition, surface-like sulfate remained at same vibrational frequency. On the contrary, bands observed over the ~1400 to ~1600 cm^{-1} range at 200 °C for Pt/Al_2O_3 sample were removed at 550 °C, which indicate that these species left the surface or were converted into other species. It should be noted that the SO_2 saturation was not achieved during the sulfur exposure at 200 °C and this can be seen by examining Figures 5 and 6, where it is clear that the intensities are increasing significantly between 90 and 120 min of exposure. However, the time for the ramping is only 17.5 min, and when comparing the large differences between the spectra at 200 and 550 °C in Figure 7, with the spectra in Figures 5 and 6 after 90 and 120 min exposure time, respectively, it is clear that the temperature plays a critical role.

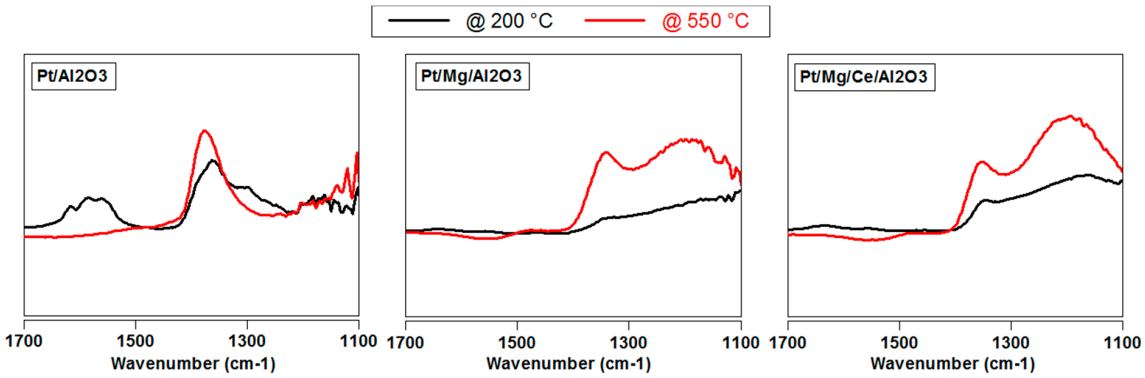

Figure 7. DRIFTS spectra for Pt/Al_2O_3, $Pt/Mg/Al_2O_3$, and $Pt/Mg/Ce/Al_2O_3$ samples after SO_2 adsorption at 200 °C and a temperature ramp at 550 °C. The reference spectrum was taken before SO_2 adsorption at 200 °C. The gas composition during adsorption and subsequent temperature ramp was 50 ppm SO_2 and 8% O_2.

Overall, the catalyst temperature clearly influences SO_2 adsorption by (a) increasing the amount of species formed (higher sulfation rate), (b) endorsing the migration of surface sulfate species to occupy more stable sulfate configurations (higher bulk-like sulfate species formed), and (c) removing weakly absorbed species during SO_2 exposure.

2.3. Sulfur Regeneration

The influence of the LNT catalyst formulation on the sulfur regeneration was investigated over nine different model LNT catalysts by performing H_2-TPR experiments. Prior to testing, the samples were sulfated in a gas feed containing 50 ppm SO_2 and 8% O_2 for 8 h at 200 °C. Table 2 numerically summarizes the results of the H_2-TPR experiment, including total H_2 consumption, and the temperatures at 20% (T20) and 90% (T90) of SO_2 released. Likewise, Figure 8 displays the resulting H_2 consumption profiles for all pre-sulfated samples. All reduction reactions involving hydrogen consumption have been reported in the Appendix A. The H_2 consumption peaks were identified as the reduction of $PdSO_4$ (peak centered at 223 °C for Pd-monometallic [39]), surface sulfites (337 °C [53]), surface aluminum sulfates (from 437 °C to 510 °C), surface magnesium/ceria sulfates (542 °C [14,54]), and bulk-like sulfates species (579 °C [38]). Surface aluminum sulfates and bulk-like sulfates were slightly shifted towards higher temperatures (+20 °C) for $Mg\text{-}Al_2O_3$ and $Mg\text{-}Ce\text{-}Al_2O_3$ samples. This is probably because of the formation of more strongly bound sulfate species in presence of Mg compared to $PGM\text{-}Al_2O_3$ samples [54]. Likewise, the reduction of surface aluminum sulfates were shifted

towards higher temperatures for the bimetallic samples. This, therefore, implies that the sulfur species formed were more stable in the bimetallic catalysts than in corresponding monometallic Pt and Pd samples. It should be also noted that the reduction of Pd-monometallic catalysts took place at lower temperatures (with lower H_2 consumption; see Table 2) with respect to other samples. For instance, the corresponding reduction peak for surface aluminum sulfates was observed at 437 °C and 480 °C for Pd- and Pt-monometallic samples, respectively. This is totally consistent with the results reported by Wilburn and Epling [34]. They found that Pd makes the formed sulfur species less strong compared to Pt containing samples due to the poor oxidizing capabilities of Pd [34].

Table 2. Summary of H_2-TPR experiment for PGM-Al_2O_3 samples tested: amount of SO_2 stored after poisoning, H_2 consumption, and temperatures at 20% (T20) and 90% (T90) of SO_2 released.

Sample	H_2 Consumption (μmol)	T20 SO_2 (°C)	T90 SO_2 (°C)
Pt/Al_2O_3	52	401	652
Pd/Al_2O_3	38.3	386.9	661.9
$Pt/Pd/Al_2O_3$	46.2	409.4	653.1
$Pt/Mg/Al_2O_3$	48.8	487.8	689.7
$Pd/Mg/Al_2O_3$	24	351.2	694.7
$Pt/Pd/Mg/Al_2O_3$	50.7	508.3	713.8
$Pt/Mg/CeO_2/Al_2O_3$	62.8	482.5	714.6
$Pd/Mg/CeO_2/Al_2O_3$	57.7	475.3	674.3
$Pt/Pd/Mg/CeO_2/Al_2O_3$	61.3	506	701.7

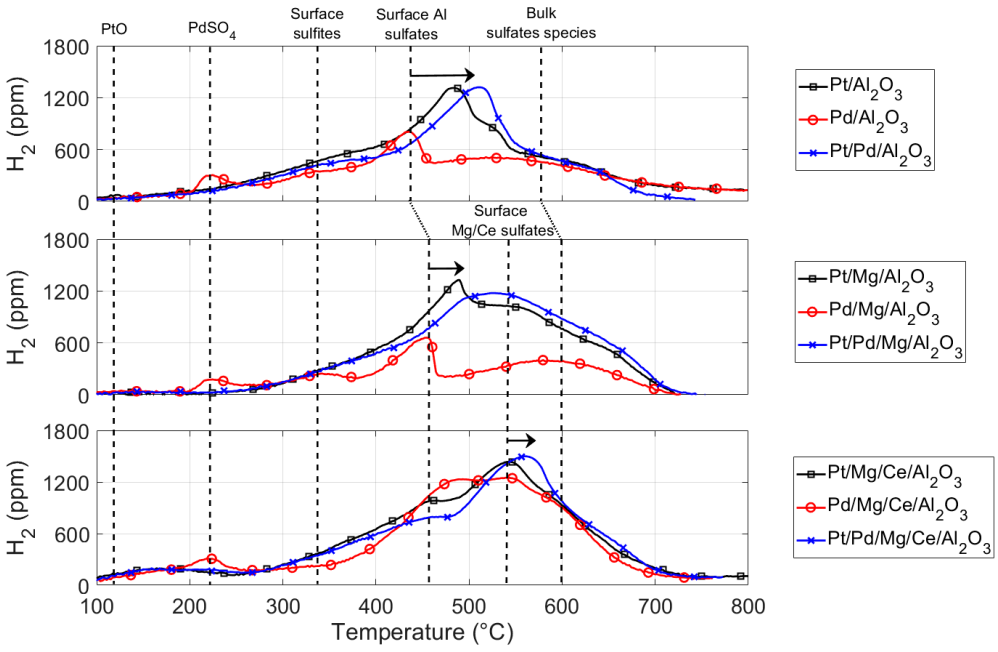

Figure 8. H_2 consumption for all samples during H_2-TPR experiment in a flow of 1600 ppm of H_2 with a ramp rate of 5 °C/min.

2.4. Temperature Programmed Desorption (TPD) after Sulfur Regeneration

In order to evaluate the effectiveness of H_2-TPR in removing sulfur species and recovering the catalytic activity, a subsequent NO_2-TPD experiment (TPD2) was carried out and compared with previous NO_2-TPD test (TPD1, before SO_2 poisoning). The samples were exposed to the same experimental procedure as in TPD1. A quantitative analysis of the amount of NO_x adsorbed and released during TPD1 and TPD2 experiments is reported in Table 3. Figure 9 compares TPD1 and TPD2 spectra for Pt/Al_2O_3, $Pd/Mg/Al_2O_3$, and $Pt/Pd/Mg/Al_2O_3$ samples during the desorption step. The amount of the total NO_x released was decreased after sulfation, ranging the reduction between

6% and 15%. This can be particularly observed for Ce containing catalysts probably because of the large formation of very stable bulk sulfates during the SO_2 exposure (according to DRIFTS spectra). Therefore, these results indicate that sulfur removal was not completely achieved during the H_2-TPR test. In fact, some SO_2 were desorbed during the temperature ramping of the TPD2 experiment, whereas a small amount of SO_2 was also released during the NO_2 exposure, implying that sulfates were probably replaced by nitrates (see Supplementary Information; see Figure S1). The remaining sulfur probably then affected the NO_x desorption performance by deactivating sites in proximity to the interface between the precious metal and Al_2O_3 support [39,49,55]. Moreover, most of the NO_x stored was desorbed as NO for all samples during TPD2, which substantially increased compared to TPD1 (except for $Pd/Mg/Al_2O_3$; see Table 3). This is probably because of the increase in the Pt-NO formation during NO_2 exposure by the oxidation of the accumulated sulfur species on the precious species [5], as presented below:

$$Pt - S + 2Pt - NO_2 \leftrightarrow Pt - SO_2 + 2Pt - NO \quad (1)$$

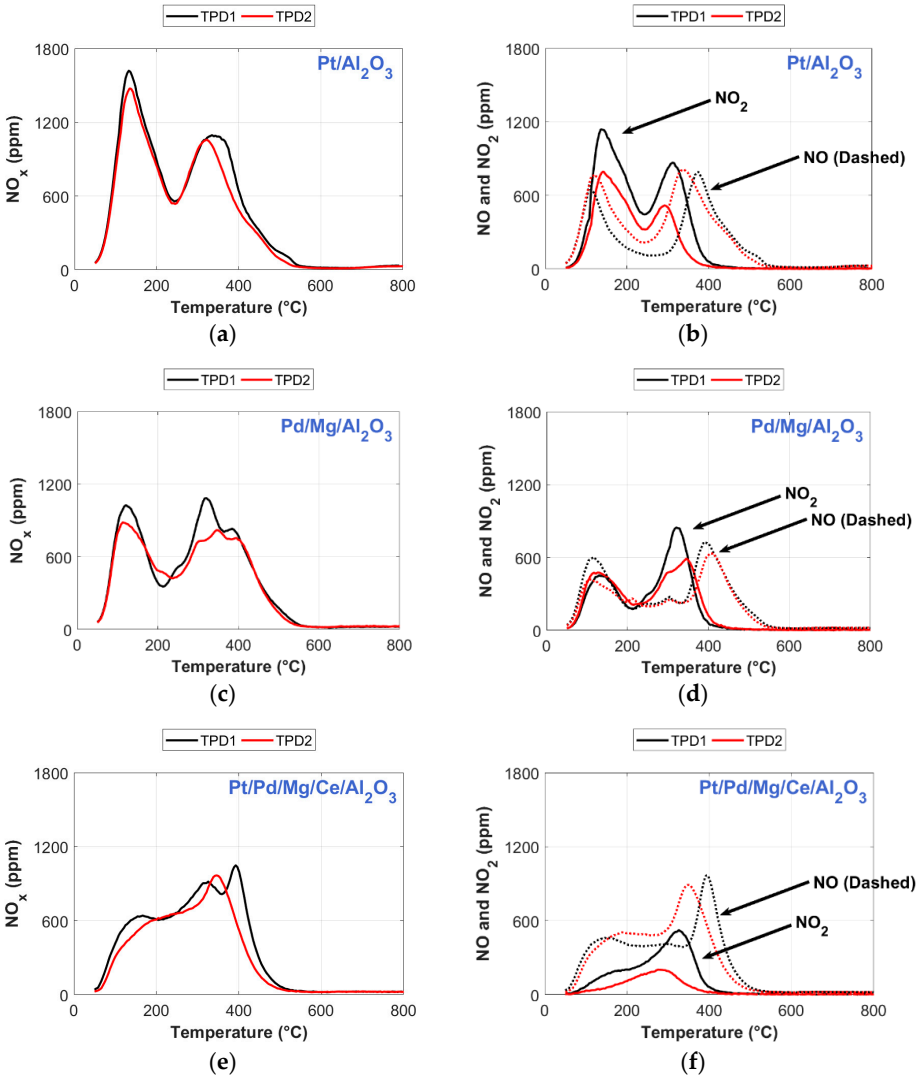

Figure 9. TPD spectra for Pt/Al_2O_3, $Pd/Mg/Al_2O_3$ and $Pt/Pd/Mg/Al_2O_3$ samples. The total NO_x release profile is shown on the left, while the NO_2 and NO release profiles are shown on the right for same group of samples. The experiments were performed before (TPD1) and after (TPD2) SO_2 poisoning. (**a**,**c**,**e**) show the total NO_x profiles (TPD1 and TPD2), and (**b**,**d**,**f**) show the NO and NO_2 profiles (TPD1 and TPD2) for Pt/Al_2O_3, $Pd/Mg/Al_2O_3$ and $Pt/Pd/Mg/Ce/Al_2O_3$ samples, respectively.

Table 3. Total NO_x adsorbed (NO_x Ads), and NO/NO_2 desorbed during temperature programmed desorption experiments performed before (TPD1) and after (TPD2) SO_2 poisoning. Note that TPD2 was performed after the temperature programmed reduction experiment.

Sample	TPD1			TPD2		
	NO_x Ads (μmol)	NO Des. (μmol)	NO_2 Des. (μmol)	NO_x Ads (μmol)	NO Des. (μmol)	NO_2 Des. (μmol)
Pt/Al_2O_3	37.3	13.8	18.2	35.7	17.4	11.3
Pd/Al_2O_3	38.9	15.6	18.1	37.4	17.5	13.1
$Pt/Pd/Al_2O_3$	37.2	11.9	20.8	36	16.1	13.9
$Pt/Mg/Al_2O_3$	35.3	15.4	11.5	34.4	16.9	7.7
$Pd/Mg/Al_2O_3$	34.5	15	11.5	34.1	13	11.1
$Pt/Pd/Mg/Al_2O_3$	37.1	17.3	10	36.8	18.8	6.9
$Pt/Mg/CeO_2/Al_2O_3$	35.5	16.6	9.4	36.7	17.9	4.2
$Pd/Mg/CeO_2/Al_2O_3$	35.8	16.8	8.7	37.2	17.5	4.1
$Pt/Pd/Mg/CeO_2/Al_2O_3$	36	17	7.5	37	17.6	3

2.5. Interpretation of the Sulfur Poisoning and Regeneration Results

An outstanding performance of $Pd/Mg/Al_2O_3$ model catalyst was clearly observed throughout this work. Its promising features include the ability to release most of the stored NO_x at reasonable temperature, the ability to release the sulfur trapped at relatively low temperatures (T90 < 700 °C), and an efficient sulfur removal with low H_2 consumption. After the temperature programmed regeneration procedure performed, the remaining sulfur on $Pd/Mg/Al_2O_3$ barely impacted the NO_x storage stability characteristics. In contrast, ceria-containing catalysts required higher temperatures for sulfur removal compared to other samples, probably caused by a large formation of very stable bulk sulfates during SO_2 poisoning procedure, as reported from DRIFTS measurements. Bounechada et al. [32] indeed suggested that the high dynamic oxygen storage capacity (OSC) of ceria-containing materials leads to the diffusion of surface sulfates into the bulk, blocking some pores and inhibiting the access to active sites. Meanwhile, the remaining sulfur species on Ce-containing catalysts certainly affected the NO_x stored stability by reducing the amount of NO_x released after sulfation.

Even though the experiments did not demonstrate a strong effect of the precious metal nature on the stability of the NO_x stored, they certainly played an important role in the sulfur poisoning and regeneration characteristics. We found that the addition of platinum on the LNT formulation facilitates the SO_2 adsorption with the formation of bulk and surface sulfate species. As discussed above, the sulfur species formed on Pt sites might quickly spill over to neighboring Al_2O_3 sites, resulting in surface aluminum sulfate formation. The resultant increase in surface aluminum sulfate might, therefore, promote the formation of very stable bulk sulfate species, observed on the DRIFTS measurements. In contrast, monometallic Pd-based catalysts barely exhibited bulk sulfate species probably because of the formation of $PdO\text{-}SO_3$ complexes, limiting the overall catalyst activity. Likewise, monometallic Pd-based catalysts exhibited better sulfur regeneration capabilities compared to other model samples tested (see Figure 8), mostly characterized by a reduced reductant consumption and lower regeneration temperatures. This is probably because Pd makes the formed sulfur species weaker compared to Pt containing samples because of the poor oxidizing capabilities of Pd. Meanwhile, bimetallic samples showed similar characteristics as the monometallic Pt-based catalysts, nevertheless more stable sulfur species were formed for Pt-Pd samples investigated. This catalytic behavior of the bimetallic samples can be attributed to the presence of electron-deficient Pt species isolated on the Pd surface [56]. These species have been reported for Pt-highly-loaded bimetallic samples (Pt > 75%) [57]. Therefore, the electron donor character of the reductant (H_2) might weaken the affinity between the Pt clusters and the reductant, resulting in a modification of the overall apparent activation energy [56].

3. Experimental

3.1. Catalyst Preparation

Nine different model catalysts were prepared using the incipient wetness impregnation method of commercial γ-Al_2O_3 (Sasol, Puralox SBa200, Brunsbüttel, Germany) and 20 wt% Ce-doped Al_2O_3 (Sasol, Puralox SCFa-160/Ce20, Brunsbüttel, Germany), both thermally treated in air at 750 °C for 4 h to remove impurities and stabilize the structure prior to impregnation. A full list of the catalysts prepared as well as their formulations is found in Table 4. All catalysts contained the same total number of precious metal (PGM) moles equivalent to 2 wt% Pt. Pt and Pd were first impregnated onto γ-Al_2O_3 and Ce-doped Al_2O_3 powders using a solution of $Pt(NO_3)_2$ (Heraeus GmbH, 14.93 wt% Pt, Hanau, Germany) and $Pd(NO_3)_2$ (Heraeus GmbH, 16.37 wt% Pd, Hanau, Germany), respectively. Samples were subsequently dried at 100 °C in air overnight and then calcined at 550 °C for 2 h.

Table 4. Component contributions by mass percent for the three groups of samples prepared: precious metals-alumina (PGM-Al_2O_3), magnesium-alumina (Mg-Al_2O_3), and magnesium-ceria- alumina (Mg-Ce-Al_2O_3).

Group	Sample	Pt	Pd	Al_2O_3	Mg	CeO_2
PGM-Al_2O_3	Pt/Al_2O_3	2	-	98	-	-
	Pd/Al_2O_3	-	1.09	98.9	-	-
	$Pt/Pd/Al_2O_3$	1.6	0.2	98.2	-	-
Mg-Al_2O_3	$Pt/Mg/Al_2O_3$	2	-	88	10	-
	$Pd/Mg/Al_2O_3$	-	1.09	88.9	10	-
	$Pt/Pd/Mg/Al_2O_3$	1.6	0.2	88.2	10	-
Mg-Ce-Al_2O_3	$Pt/Mg/CeO_2/Al_2O_3$	2	-	68	10	20
	$Pd/Mg/CeO_2/Al_2O_3$	-	1.09	68.9	10	20
	$Pt/Pd/Mg/CeO_2/Al_2O_3$	1.6	0.2	68.2	10	20

Bimetallic samples were prepared by sequential wet impregnation of Pt and Pd based on a commercial LNT catalyst with a Pt/Pd ratio of 80% Pt and 20% Pd [2]. First, 1.6 wt% Pt/Al_2O_3 was prepared as described above in the case of monometallic samples. After calcination at 550 °C for 2 h, a solution containing the palladium precursor was prepared and added drop-wise to the catalyst powder. The catalyst was subsequently dried and calcined at 550 °C for 2 h.

Catalysts containing 10 wt% Mg were then prepared by a dilution of $C_4H_6MgO_4 \cdot 4H_2O$ (Sigma-Aldrich, St. Louis, MO, USA) in milliQ water. The precursor solution was added drop-wise to PGM/γ-Al_2O_3 and PGM/Ce-Al_2O_3 slurries followed by drying in air overnight at 100 °C and calcining at 550 °C for 2 h.

3.2. Catalytic Evaluation Experiments

The catalytic evaluation experiments were conducted in a vertical quartz tube mounted in an electric furnace as a part of Setaram Sensys DSC instrument (Digital Scanning Calorimeter, Caluire, France). The catalyst powder (~70 mg) was placed inside the tube on a porous quartz bed. A flow of 20 mL/min was sent into the catalyst-containing tube and the gases were taken from a larger gas flow to enhance the transient response of the system. Multiple mass flow controllers (Bronkhorst Hi-Tech Low-ΔP Flow, Ruurlo, Netherlands) were employed to control the inlet gas composition, whereas the outlet gas composition was analyzed with a Hiden HPR-20QUI mass spectrometer (MS): NO (m/z = 30), NO_2 (m/z = 46), H_2 (m/z = 2), O_2 (m/z = 32), SO_2 (m/z = 64), and Ar (m/z = 20). The NO–NO_2 spectral interference was considered for the data analysis. Calibration curves were collected before each experiment for the quantitative analysis using diluted gaseous mixtures. All experiments were carried out in nearly isothermal conditions at atmospheric pressure with Ar balance. Prior to testing, all samples were pre-treated at 500 °C for 1 h in a flow containing 2% H_2. The experimental campaign consisted of NO_2-temperature programmed desorption and H_2-temperature programmed reduction

experiments, which are described in detail below. It is important to remark that the experimental campaign was conducted in the absence of CO_2 and water. It is well known that the presence of H_2O and CO_2 in the exhaust stream have an effect on the catalyst surface and consequently on the reaction chemistry. We have used these conditions in order to facilitate the comparison between NO_x and SO_x interactions.

3.2.1. NO_2-TPD Experiments

NO_2 temperature programmed desorption (NO_2-TPD) experiments were carried out to compare the thermal stability of NO_x stored species among the catalysts prepared. The samples were first exposed to 900 ppm NO_2 for 1 h at 50 °C and then flushed in Ar for 30 min. The temperature was subsequently increased to 800 °C with a ramp rate of 10 °C/min in Ar. The experimental procedure is also illustrated in Figure 10 for Pt/Al_2O_3.

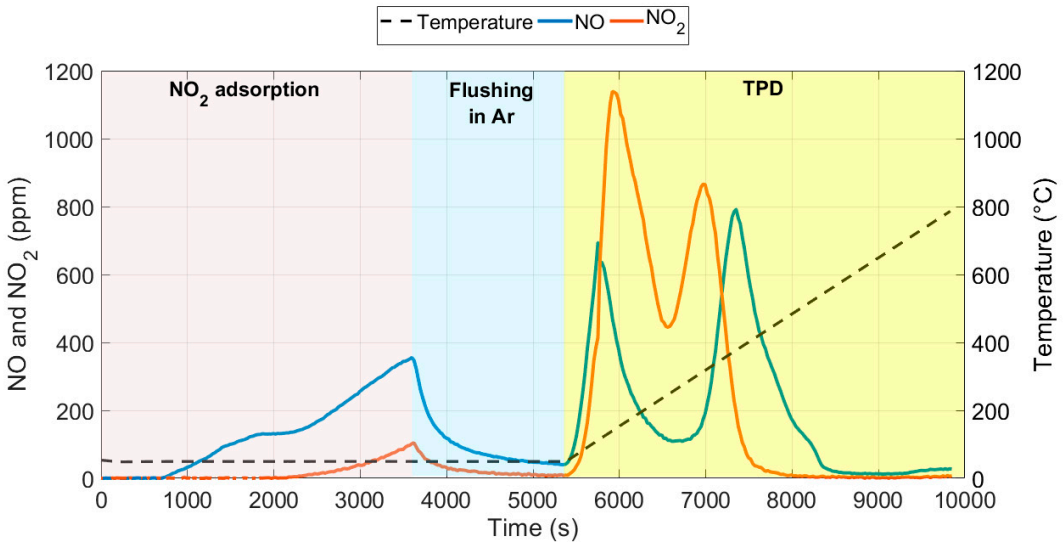

Figure 10. Reaction protocol for TPD experiment for Pt/Al_2O_3.

Same experimental procedure was repeated over all samples after SO_2 poisoning and H_2-TPR experiments (described below) in order to evaluate the effectiveness of H_2-TPR in removing sulfur species and recovering the catalytic activity by comparing both NO_2-TPD results.

3.2.2. SO_2 Poisoning and H_2-TPR Experiments

Hydrogen temperature programmed reduction experiments were conducted over the model catalysts in order to examine the stability of sulfur species stored during a SO_2 poisoning procedure. The samples were first subjected to 50 ppm SO_2 and 3% O_2 for 8 h at 200 °C. The temperature was then decreased to 50 °C in presence of Ar. Thereafter, a flow containing 1600 ppm of H_2 was introduced for 1 h at 50 °C, followed by increasing the temperature to 800 °C with a ramp rate of 5 °C/min in presence of H_2. The temperature was subsequently maintained constant at 800 °C for 30 min in 1600 ppm of H_2.

3.3. DRIFT Spectroscopy

In situ FTIR spectroscopy experiments were conducted in diffusive reflectance mode (DRIFTS) to follow the evolution of surface species during SO_2 poisoning. The experiment set-up consisted of a BRUKER Vertex 70 spectrometer (Billerica, MA, USA) equipped with a Harrick Praying Mantis DR stainless steel reaction cell and a nitrogen-cooled MCT detector. The reaction cell contains a sample cup with a porous grid, where approximately 70 mg of catalysts powder was placed. The sample was then covered by a dome equipped with two ZnSe windows. The feed gases were flown through the sample via separate mass flow controllers (Bronkhorst Hi-Tech Low- ΔP Flow, Ruurlo, Netherlands),

providing a total gas flow of 100 mL/min for all experiments. All samples were pretreated in 1% H_2 at 500 °C for 1 h and then exposed to 3% O_2 for 10 min. Thereafter, the temperature was reduced to 200 °C in Ar flow and a background spectrum was collected. The feed gas was then switched to 50 ppm SO_2 and 3% O_2 for 2 h at 200 °C. During this time, infrared spectra were acquired every 60 s between 650 and 4000 cm^{-1} with a spectral resolution of 2 cm^{-1}.

The evolution and stability of sulfur species were then evaluated for Pt/Al_2O_3, $Pt/Mg/Al_2O_3$, and $Pt/Mg/Ce/Al_2O_3$ samples during a temperature ramp. Immediately after SO_2 poisoning, the temperature was raised from 200 °C to 550 °C at a rate of 20 °C/min in a feed containing 50 ppm of SO_2 and 8% O_2. DRIFTS spectra were collected every 60 s during the temperature ramp, and then subtracted to the background spectrum collected before SO_2 poisoning at 200 °C.

4. Conclusions

A comparable investigation among nine different LNT model catalysts were performed with the purpose of studying the sulfur poisoning and regeneration characteristics on modern LNT components. The model samples consisted of three compounds: (i) Al_2O_3, (ii) Mg/Al_2O_3, and (iii) $Mg/Ce/Al_2O_3$ mixed with Pt, Pd, and Pt-Pd. Temperature programmed reaction and DRIFTS spectroscopy results showed that palladium and magnesium are key components in the development of modern LNT catalysts. They provide appropriate NO_x release temperature range, outstanding regeneration capabilities, and low reductant consumption. This was especially evident for $Pd/Mg/Al_2O_3$ sample, which presented an excellent performance during the testing campaign performed. However, monometallic Pd-based catalysts exhibited the formation of surface palladium sulfate species during SO_2 exposure, which might limit the catalytic performance of the catalyst. Alternatively, it was therefore suggested that Pt-Pd bimetallic formulations could provide some improvements of the catalytic behavior of monometallic Pd catalysts since the formation of surface palladium sulfate was not observed during SO_2 exposure. However, the higher stability of sulfur species was observed for the bimetallic samples investigated. Furthermore, it was found that the addition of ceria into LNT formulations leads to the increased formation of bulk sulfate species. This is probably because of the high dynamic oxygen storage capacity property of ceria-containing materials which results in the diffusion of surface sulfates into the bulk.

Supplementary Materials: The following are available online at http://www.mdpi.com/2073-4344/9/6/492/s1, Figure S1: SO_2 desorption profile during TPD2 for Pt/Al_2O_3.

Author Contributions: Conceptualization, J.E.D.A.G., A.K. and L.O.; Methodology, J.E.D.A.G. and L.O.; Data Acquisition, J.E.D.A.G.; Data Analysis, J.E.D.A.G. and L.O.; Writing—original draft, J.E.D.A.G.; Writing—Review & Editing, J.E.D.A.G., A.K. and L.O.; and Supervision, A.K. and L.O.

Acknowledgments: This study is a collaboration between Volvo Car Corporation and Competence Centre for Catalysis at Chalmers University of Technology. We gratefully acknowledge the financial support from Volvo Car Corporation and the Swedish Foundation for Strategic Research (ID15-0030).

Conflicts of Interest: The authors declare no conflict of interest.

Appendix A

The reduction reactions that involved hydrogen consumption are reported below:

$$M-SO_4+4H_2 \rightarrow M-O+H_2S+3H_2O \quad [47] \quad (A1)$$

$$M-SO_4+3H_2 \rightarrow M-O+SO_2+3H_2O \quad [8] \quad (A2)$$

$$M-SO_4+4H_2 \rightarrow M-S+4H_2O \quad [47] \quad (A3)$$

$$M-S+H_2O \rightarrow M-O+H_2S \quad [47] \quad (A4)$$

$$M-SO_2+3H_2 \rightarrow M-O+H_2S+2H_2O \quad [8] \quad (A5)$$

where *M* denotes metal oxides as SO_x absorbents. Likewise, the reduction reaction for the precious metals is:

$$PGM-SO_2+PGM+H_2 \rightarrow 2PGM-O+H_2S \quad [5] \quad (A6)$$

References

1. Ottinger, N.A.; Toops, T.J.; Pihl, J.A.; Roop, J.T.; Choi, J.-S.; Partridge, W.P. Sulfate storage and stability on representative commercial lean NO_x trap components. *Appl. Catal. B Environ.* **2012**, *117–118*, 167–176. [CrossRef]
2. De Abreu Goes, J.E.; Olsson, L.; Berggrund, M.; Kristoffersson, A.; Gustafson, L.; Hicks, M. Performance Studies and Correlation between Vehicle- and Rapid-Aged Commercial Lean NO_x Trap Catalysts. *SAE Int. J. Engines* **2017**, *10*, 1613–1626. [CrossRef]
3. Johnson, T.; Joshi, A. Review of Vehicle Engine Efficiency and Emissions. *SAE Int. J. Engines* **2018**, *11*, 1307–1330. [CrossRef]
4. Choi, J.-S.; Partridge, W.P.; Pihl, J.A.; Daw, C.S. Sulfur and temperature effects on the spatial distribution of reactions inside a lean NO_x trap and resulting changes in global performance. *Catal. Today* **2008**, *136*, 173–182. [CrossRef]
5. Dawody, J.; Skoglundh, M.; Olsson, L.; Fridell, E. Kinetic modelling of sulfur deactivation of $Pt/BaO/Al_2O_3$ and BaO/Al_2O_3 NO_x storage catalysts. *Appl. Catal. B Environ.* **2007**, *70*, 179–188. [CrossRef]
6. Liu, Y.; He, H.; Xu, W.; Yu, Y. Mechanism of Heterogeneous Reaction of Carbonyl Sulfide on Magnesium Oxide. *The J. Phys. Chem. A* **2007**, *111*, 4333–4339. [CrossRef] [PubMed]
7. Rohr, F.; Göbel, U.; Kattwinkel, P.; Kreuzer, T.; Müller, W.; Philipp, S.; Gélin, P. New insight into the interaction of sulfur with diesel NO_x storage catalysts. *Appl. Catal. B Environ.* **2007**, *70*, 189–197. [CrossRef]
8. Lafossas, F.-A.; Manetas, C.; Mohammadi, A.; Kalogirou, M.; Koltsakis, G.; Samaras, Z.; Iida, M.; Inoue, M. Sulfation and Lean/Rich Desulfation of a NO_x storage Reduction Catalyst: Experimental and Simulation Study. *Int. J. Engine Res.* **2015**, *16*, 197–212. [CrossRef]
9. Hadl, K.; Ratzberger, R.; Eichlseder, H.; Schuessler, M.; Linares, W.; Pucher, H. Sulfur Poisoning of a NOx Storage Catalyst—A Comprehensive Modelling Approach. *SAE Int. J. Engines* **2016**. [CrossRef]
10. Olsson, L.; Blint, R.J.; Fridell, E. Global Kinetic Model for Lean NO_x Traps. *Ind. Eng. Chem. Res.* **2005**, *44*, 3021–3032. [CrossRef]
11. AL-Harbi, M.; Epling, W.S. Investigating the Effect of NO Versus NO_2 on the Performance of a Model NO_x Storage/Reduction Catalyst. *Catal. Lett.* **2009**, *130*, 121–129. [CrossRef]
12. Benramdhane, S.; Millet, C.-N.; Jeudy, E.; Lavy, J.; Blasin-Aubé, V.; Daturi, M. Diesel Lean NO_x-Trap Thermal Aging and Performance Evolution Characterization. *Oil Gas Sci. Technol. Rev. IFP Energies nouvelles* **2011**, *66*, 845–853. [CrossRef]
13. Rohr, F.; Peter, S.D.; Lox, E.; Kögel, M.; Sassi, A.; Juste, L.; Rigaudeau, C.; Belot, G.; Gélin, P.; Primet, M. On the Mechanism of Sulphur Poisoning and Regeneration of a Commercial Gasoline NO_x-Storage Catalyst. *Appl. Catal. B Environ.* **2005**, *56*, 201–212. [CrossRef]
14. Ji, Y.; Toops, T.J.; Crocker, M. Effect of Ceria on the Sulfation and Desulfation Characteristics of a Model Lean NO x Trap Catalyst. *Catal. Lett.* **2009**, *127*, 55–62. [CrossRef]
15. Easterling, V.; Ji, Y.; Crocker, M.; Ura, J.; Theis, J.R.; McCabe, R.W. Effect of ceria on the desulfation characteristics of model lean NO_x trap catalysts. *Catal. Today* **2010**, *151*, 338–346. [CrossRef]
16. Choi, J.-S.; Partridge, W.P.; Lance, M.J.; Walker, L.R.; Pihl, J.A.; Toops, T.J.; Finney, C.E.A.; Daw, C.S. Nature and Spatial Distribution of Sulfur Species in a Sulfated Barium-Based Commercial Lean NO_x Trap Catalyst. *Catal. Today* **2010**, *151*, 354–361. [CrossRef]
17. Basile, F.; Fornasari, G.; Gambatesa, A.; Livi, M.; Vaccari, A. Reactivity of Mg-Ba catalyst in NO_x storage/reduction. *Catal. Today* **2007**, *119*, 59–63. [CrossRef]
18. Jeong, S.; Youn, S.; Kim, D.H. Effect of Mg/Al ratios on the NO_x storage activity over Pt-BaO/Mg–Al mixed oxides. *Catal. Today* **2014**, *231*, 155–163. [CrossRef]
19. Luo, J.; Gao, F.; Karim, A.M.; Xu, P.; Browning, N.D.; Peden, C.H.F. Advantages of MgAlOx over γ-Al_2O_3 as a Support Material for Potassium-Based High-Temperature Lean NO_x Traps. *ACS Catal.* **2015**, *5*, 4680–4689. [CrossRef]
20. Nova, I.; Castoldi, L.; Prinetto, F.; Dal Santo, V.; Lietti, L.; Tronconi, E.; Forzatti, P.; Ghiotti, G.; Psaro, R.; Recchia, S. NO_x Adsorption Study over Pt–Ba/Alumina Catalysts: FT-IR and Reactivity Study. *Top. Catal.* **2004**, *30*, 181–186. [CrossRef]
21. Scotti, A.; Nova, I.; Tronconi, E.; Castoldi, L.; Lietti, L.; Forzatti, P. Kinetic Study of Lean NO_x Storage over the Pt−Ba/Al2O3 System. *Ind. Eng. Chem. Res.* **2004**, *43*, 4522–4534. [CrossRef]

22. Forzatti, P.; Castoldi, L.; Lietti, L.; Nova, I.; Tronconi, E. Chapter 6 Identification of the reaction networks of the NOx storage/reduction in lean NOx trap systems. In *Studies in Surface Science and Catalysis*; Granger, P., Pârvulescu, V.I., Eds.; Elsevier: Amsterdam, The Netherlands, 2007; Volume 171, pp. 175–208.
23. Lietti, L.; Daturi, M.; Blasin-Aubé, V.; Ghiotti, G.; Prinetto, F.; Forzatti, P. Relevance of the Nitrite Route in the NO_x Adsorption Mechanism over Pt–Ba/Al_2O_3 NO_x Storage Reduction Catalysts Investigated by using Operando FTIR Spectroscopy. *ChemCatChem* **2012**, *4*, 55–58. [CrossRef]
24. Prinetto, F.; Ghiotti, G.; Nova, I.; Lietti, L.; Tronconi, E.; Forzatti, P. FT-IR and TPD Investigation of the NO_x Storage Properties of BaO/Al_2O_3 and Pt–BaO/Al_2O_3 Catalysts. *J. Phys. Chem. B* **2001**, *105*, 12732–12745. [CrossRef]
25. Lindholm, A.; Currier, N.W.; Dawody, J.; Hidayat, A.; Li, J.; Yezerets, A.; Olsson, L. The influence of the preparation procedure on the storage and regeneration behavior of Pt and Ba based NO_x storage and reduction catalysts. *Appl. Catal. B Environ.* **2009**, *88*, 240–248. [CrossRef]
26. Svedberg, P.; Jobson, E.; Erkfeldt, S.; Andersson, B.; Larsson, M.; Skoglundh, M. Influence of the storage material on the storage of NO x at low temperatures. *Top. Catal.* **2004**, *30*, 199–206. [CrossRef]
27. De Abreu Goes, J.; Kristoffersson, A.; Wentworth, T.; Olsson, L. Detailed Characterization Studies of Vehicle and Rapid Aged Commercial Lean NO_x Trap Catalysts. *Ind. Eng. Chem. Res.* **2018**. [CrossRef]
28. Uy, D.; Wiegand, K.A.; O'Neill, A.E.; Dearth, M.A.; Weber, W.H. In Situ UV Raman Study of the NO_x Trapping and Sulfur Poisoning Behavior of Pt/Ba/γ-Al_2O_3 Catalysts. *J. Phys. Chem. B* **2002**, *106*, 387–394. [CrossRef]
29. Abdulhamid, H.; Fridell, E.; Dawody, J.; Skoglundh, M. In situ FTIR study of SO_2 interaction with Pt/$BaCO_3$/Al_2O_3 NO_x storage catalysts under lean and rich conditions. *J. Catal.* **2006**, *241*, 200–210. [CrossRef]
30. Waqif, M.; Saur, O.; Lavalley, J.C.; Perathoner, S.; Centi, G. Nature and mechanism of formation of sulfate species on copper/alumina sorbent-catalysts for sulfur dioxide removal. *J. Phys. Chem.* **1991**, *95*, 4051–4058. [CrossRef]
31. Xie, S.X.; Yu, Y.B.; Wang, J.; He, H. Effect Of SO_2 on the performance of Ag-Pd/Al_2O_3 for the selective catalytic reduction of NO_x with C_2H_5OH. *J. Environ. Sci.* **2006**, *18*, 973–978. [CrossRef]
32. Bounechada, D.; Fouladvand, S.; Kylhammar, L.; Pingel, T.; Olsson, E.; Skoglundh, M.; Gustafson, J.; Di Michiel, M.; Newton, M.A.; Carlsson, P.-A. Mechanisms behind sulfur promoted oxidation of methane. *Phys. Chem. Chem. Phys.* **2013**, *15*, 8648–8661. [CrossRef] [PubMed]
33. Mitchell, M.B.; Sheinker, V.N.; White, M.G. Adsorption and Reaction of Sulfur Dioxide on Alumina and Sodium-Impregnated Alumina. *J. Phys. Chem.* **1996**, *100*, 7550–7557. [CrossRef]
34. Wilburn, M.S.; Epling, W.S. SO_2 adsorption and desorption characteristics of bimetallic Pd-Pt catalysts: Pd:Pt ratio dependency. *Catal. Today* **2017**. [CrossRef]
35. Li, Y.; Shen, M.; Wang, J.; Wan, T.; Wang, J. Influence of sulfation and regeneration on Pt/Al_2O_3 for NO oxidation. *Catal. Sci. Technol.* **2015**, *5*, 1731–1740. [CrossRef]
36. Mowery, D.L.; McCormick, R.L. Deactivation of alumina supported and unsupported PdO methane oxidation catalyst: the effect of water on sulfate poisoning. *Appl. Catal. B Environ.* **2001**, *34*, 287–297. [CrossRef]
37. Yu, T.-C.; Shaw, H. The effect of sulfur poisoning on methane oxidation over palladium supported on γ-alumina catalysts. *Appl. Catal. B Environ.* **1998**, *18*, 105–114. [CrossRef]
38. Colussi, S.; Arosio, F.; Montanari, T.; Busca, G.; Groppi, G.; Trovarelli, A. Study of sulfur poisoning on Pd/Al_2O_3 and Pd/CeO_2/Al_2O_3 methane combustion catalysts. *Catal. Today* **2010**, *155*, 59–65. [CrossRef]
39. Wilburn, M.S.; Epling, W.S. Sulfur deactivation and regeneration of mono- and bimetallic Pd-Pt methane oxidation catalysts. *Appl. Catal. B Environ.* **2017**, *206*, 589–598. [CrossRef]
40. Lampert, J.K.; Kazi, M.S.; Farrauto, R.J. Palladium catalyst performance for methane emissions abatement from lean burn natural gas vehicles. *Appl. Catal. B Environ.* **1997**, *14*, 211–223. [CrossRef]
41. Ohtsuka, H. The selective catalytic reduction of nitrogen oxides by methane on noble metal-loaded sulfated zirconia. *Appl. Catal. B Environ.* **2001**, *33*, 325–333. [CrossRef]
42. Gélin, P.; Primet, M. Complete oxidation of methane at low temperature over noble metal based catalysts: A review. *Appl. Catal. B Environ.* **2002**, *39*, 1–37. [CrossRef]
43. Lapisardi, G.; Gélin, P.; Kaddouri, A.; Garbowski, E.; Da Costa, S. Pt–Pd bimetallic catalysts for methane emissions abatement. *Top. Catal.* **2007**, *42*, 461–464. [CrossRef]
44. Sadokhina, N.; Smedler, G.; Nylén, U.; Olofsson, M.; Olsson, L. Deceleration of SO_2 poisoning on PtPd/Al2O3 catalyst during complete methane oxidation. *Appl. Catal. B Environ.* **2018**, *236*, 384–395. [CrossRef]

45. Knözinger, H.; Ratnasamy, P. Catalytic Aluminas: Surface Models and Characterization of Surface Sites. *Catal. Rev.* **1978**, *17*, 31–70. [CrossRef]
46. Hamzehlouyan, T.; Sampara, C.S.; Li, J.; Kumar, A.; Epling, W.S. Kinetic study of adsorption and desorption of SO_2 over γ-Al_2O_3 and Pt/γ-Al_2O_3. *Appl. Catal. B Environ.* **2016**, *181*, 587–598. [CrossRef]
47. Wang, J.-A.; Li, C.-L. SO_2 adsorption and thermal stability and reducibility of sulfates formed on the magnesium–aluminate spinel sulfur-transfer catalyst. *Appl. Surf. Sci.* **2000**, *161*, 406–416. [CrossRef]
48. Schneider, W.F.; Li, J.; Hass, K.C. Combined Computational and Experimental Investigation of SO_x Adsorption on MgO. *J. Phys. Chem. B* **2001**, *105*, 6972–6979. [CrossRef]
49. Kylhammar, L.; Carlsson, P.-A.; Skoglundh, M. Sulfur promoted low-temperature oxidation of methane over ceria supported platinum catalysts. *J. Catal.* **2011**, *284*, 50–59. [CrossRef]
50. Kylhammar, L.; Carlsson, P.-A.; Ingelsten, H.H.; Grönbeck, H.; Skoglundh, M. Regenerable ceria-based SO_x traps for sulfur removal in lean exhausts. *Appl. Catal. B Environ.* **2008**, *84*, 268–276. [CrossRef]
51. Li, J.; Theis, J.; Chun, W.; Goralski, C.; Kudla, R.; Ura, J.; Watkins, W.; Chattha, M.; Hurley, R. Sulfur Poisoning and Desulfation of the Lean NO_x Trap. *SAE Tech. Pap.* **2001**. [CrossRef]
52. Boaro, M.; de Leitenburg, C.; Dolcetti, G.; Trovarelli, A.; Graziani, M. Oxygen Storage Behavior of Ceria–Zirconia-Based Catalysts in the Presence of SO_2. *Top. Catal.* **2001**, *16*, 299–306. [CrossRef]
53. Hamzehlouyan, T.; Sampara, C.; Li, J.; Kumar, A.; Epling, W. Sulfur Poisoning of a Pt/Al_2O_3 Oxidation Catalyst: Understanding of SO_2, SO_3 and H_2SO_4 Impacts. *Top. Catal.* **2016**, *59*, 1028–1032. [CrossRef]
54. Jeong, S.; Kim, D.H. Sulfation and Desulfation Behavior of Pt-BaO/MgO-Al_2O_3 NO_x Storage Reduction Catalyst. *J. Nanosci. Nanotechnol.* **2016**, *16*, 4411–4416. [CrossRef] [PubMed]
55. Epling, W.S.; Campbell, L.E.; Yezerets, A.; Currier, N.W.; Parks, J.E. Overview of the Fundamental Reactions and Degradation Mechanisms of NO_x Storage/Reduction Catalysts. *Catal. Rev.* **2004**, *46*, 163–245. [CrossRef]
56. Navarro, R.M.; Pawelec, B.; Trejo, J.M.; Mariscal, R.; Fierro, J.L.G. Hydrogenation of Aromatics on Sulfur-Resistant PtPd Bimetallic Catalysts. *J. Catal.* **2000**, *189*, 184–194. [CrossRef]
57. Rades, T.; Pak, C.; Polisset-Thfoin, M.; Ryoo, R.; Fraissard, J. Characterization of bimetallic NaY-supported Pt-Pd catalyst by EXAFS, TEM and TPR. *Catal. Lett.* **1994**, *29*, 91–103. [CrossRef]